DNA-controlled Spatio-temporal Patterning of Active Matter

Yuliia Vyborna*, Jean-Christophe Galas*, and André Estevez-Torres*

Sorbonne Université, CNRS, Institut de Biologie Paris-Seine (IBPS), Laboratoire Jean Perrin (LJP), F-75005, Paris, France

Corresponding Authors

Yuliia Vyborna − Email: yuliia.vyborna@sorbonne-universite.fr
Jean-Christophe Galas − Email: jean-christophe.galas@upmc.fr
André Estevez-Torres − Email: andre.estevez-torres@sorbonne-universite.fr

ABSTRACT: Molecular programs and active matter appear as two key ingredients for the emergence of shape in living systems. The former process chemical information, while the latter generates long-range mechanical forces. The coupling of these two elements is thus essential for the synthesis of life-like materials. Here, we describe the preparation of DNA-responsive surfaces that shape a cm-scale tridimensional active gel comprised of microtubules: a DNA signal triggers the gel, structuring it into a periodic band pattern or local aggregates, depending on its sequence and concentration. Finally, we show how a gradient of DNA concentration transfers its positional information to the active gel, mimicking chemo-mechanical patterning promoted by morphogens during embryo development. We anticipate that such DNA-controlled active matter will contribute to the development of life-like materials with self-shaping properties

From a chemist's perspective, a living embryo can be regarded as a material that self-organizes in shape and composition following a complex series of physicochemical transformations.[1,2] To drive these transformations, chemistry and mechanics are intimately coupled: while chemical reaction networks process molecular information, mechanical processes generate forces and flows that change the macroscopic shape. Their combination is thus a necessary step for the development of life-like synthetic materials.[3,4] However, engineering such a chemo-mechanical coupling in vitro remains challenging. A promising route relies on DNA hybridization reactions triggering forces that can be mechanically amplified to produce shape changes at the macroscopic scale. Indeed, DNA reactions can be exquisitely controlled,[5] assembled into logical[6,7] and out-of-equilibrium chemical programs,[8–11] and coupled to a great variety of materials.[12–16] The mechanical amplification of a DNA signal can be either performed by DNA reactions, such as in DNA-responsive hydrogels,[17,18] or by motor proteins, such as in DNA-responsive cytoskeletal active matter.[19–21] While DNA reactions have the advantage of greater programmability, they lack the self-organization properties of active matter.[22–25] Thus far, no methods have been developed to make a DNA-responsive active matter able to self-organize at the macro-scale, yet the realization of such a system could open opportunities to life-like self-patterned materials.

In this paper, we introduce a new type of DNA-responsive cytoskeletal active matter that self-organizes over a centimeter scale. Active gels composed of clustered kinesin motors and microtubule filaments are capable of spontaneous motion[23] and self-organization into a variety of patterns that, in some cases, induce flow and shape changes at the centimeter scale.[26,27] To control the activity of such gels with a DNA signal, we exploited the approach based on the spatial separation of the gel's components that are brought together on-demand by a specific DNA input (**I** DNA). Specifically, kinesin clusters were attached to the DNA-modified surface of a glass channel using biotin-streptavidin interaction and DNA hybridization.[28,29] Motor clusters were released to the medium solely after the addition of **I** (Fig. 1A). Upon attachment to the neighboring microtubules, clustered kinesins caused the macroscale local contraction of the active gel. Furthermore, when the input DNA strand was heterogeneously distributed, it acted as a morphogen and determined pattern formation in the active gel depending on the DNA concentration gradient. Thus, this system paves the way toward the on-demand shaping of soft matter guided by DNA.

To prepare densely-covered DNA glass surfaces, acrylamide and acrydite-DNA **S** were copolymerized onto silanized glass slides (SI).[30] These DNA-modified slides were further used to fabricate rectangular channels with typical dimensions of 22 × 1.5 × 0.1 mm^3. Then, a solution of biotin-labeled target DNA **T** was added to the channel to form duplex **S**:**T** on the surface due to their partial complementarity (Fig. 1B). Second, streptavidin (**str**) was injected into the channel and conjugated with biotinylated **T**, generating complex **S**:**T**:**str**. Considering that **T** bears a single biotin and that streptavidin was added in 10-fold excess, the formation of 1:1 **T**:**str** complexes with three free biotin-binding sites in the streptavidin was expected. Finally, biotinylated kinesin (**kin**) was flown inside the channel to form **S**:**T**:**str**:$\mathbf{kin_n}$ with a **kin**/**str** ratio, n, that varied between 1 and 3. This resulted in kinesin clusters attached to the surface and distributed throughout the channel. Fluorescently labeled streptavidin was used to estimate the surface density of motor clusters that could be changed from 3×10^8 to 2×10^{10} molecules/cm^2 (SI Fig. S1). The non-specific attachment of **T**, **str** and **kin** to the surface was minimized in the presence of a 2% solution of Pluronic F-127 (SI Fig. S2).

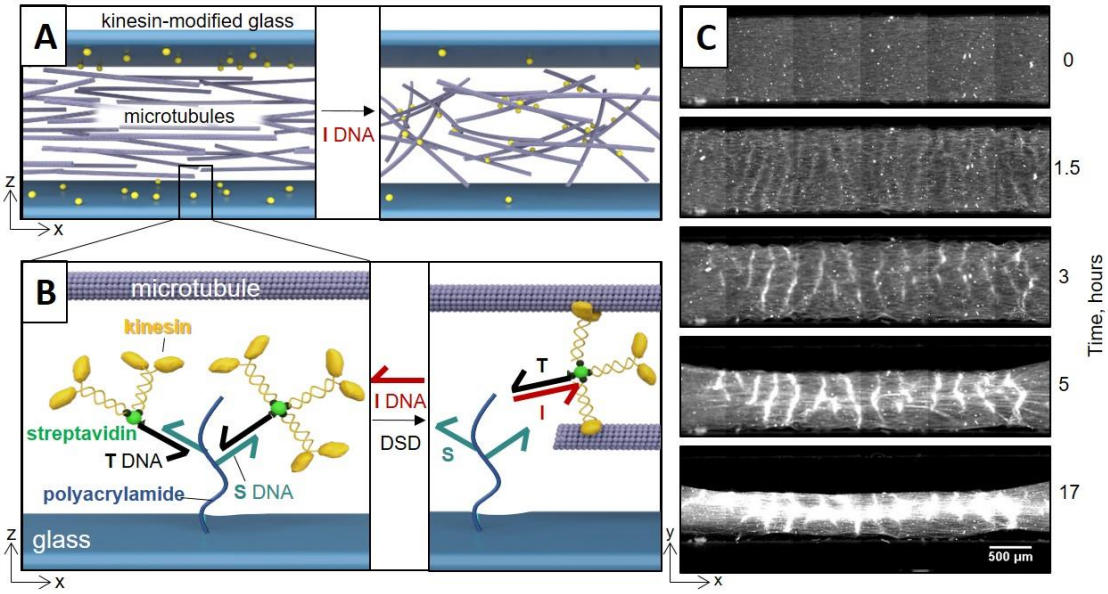

Figure 1. DNA-responsive, motor-decorated surfaces control the patterning of a cytoskeletal active gel. A: Schematic representation of a channel filled with microtubules. Glass surfaces (in blue) are modified with kinesin-DNA constructs (yellow spheres). Upon addition of strand **I**, the motors are released into the bulk inducing forces upon the microtubules. B: Schematic representation of a glass surface functionalized by DNA/polyacrylamide brushes with kinesin–streptavidin-DNA constructs attached through DNA hybridized strands that undergo toehold-mediated strand displacement reaction. An invading strand **I** binds and displaces **T** DNA, releasing kinesin-streptavidin-DNA constructs. C: Time-lapse fluorescent microscopy images of the microtubule solution confined in glass channels in the presence of 1 µM of **I** DNA. For detailed conditions see SI.

The kinesin-decorated channel was subsequently filled with a solution of microtubules (Fig. 1A) self-assembled into bundles in the presence of the depletion agent Pluronic.[23] The microtubules in the bulk and the kinesins on the surface were physically separated and the gel remained immobile for tens of hours (Movie S1). The detachment of kinesin clusters from the surface was achieved through a DNA strand displacement (DSD) reaction in the presence of the invader strand **I** that is fully complementary to **T** (Fig. 1B).[31] We thus have

$$\mathbf{S}:\mathbf{T}:\mathbf{str}:\mathbf{kin}_n + \mathbf{I} \underset{k_{-1}}{\overset{k_1}{\rightleftharpoons}} \mathbf{S} + \mathbf{I}:\mathbf{T}:\mathbf{str}:\mathbf{kin}_n \qquad (1)$$

where the formation of the duplex **I**:**T** is thermodynamically favored compared to **S**:**T** because the former is 5 base-pairs longer than the latter. Fig. 1C and Movie S1 show the behavior of the gel in the presence of 1 µM of **I**. Within five hours, the gel contracted along the *x* and *y* axis to form bright bands parallel to the *y* axis with a typical period of 300 ± 50 µm. The structure appearing in the early stages of the activity, ca. 1.5 hours, is reminiscent of the corrugations observed in a similar system where the kinesin clusters were initially present in solution.[27] Noteworthy, the initial nematic state of the microtubule gel remained virtually unchanged in the absence of **I**, or in the presence of a DNA strand with a random sequence (**N**), (Fig. S3 and Movie S1). These observations are compatible with reaction (1), indicating that DNA releases kinesin clusters into the medium, inducing the mutual sliding of the bundles and shaping the active gel at the centimiter scale.

We measured the kinetics and thermodynamics of the forward reaction (1) by following the fluorescence from labeled-streptavidin on the glass surfaces. Fig. 2A shows that the characteristic time for releasing **I**:**T**:**str**:**kin**$_n$ from the surface is equal to 5.5 min when [**I**] = 1 µM and thus the corresponding rate constant is $k_1 = 3 \times 10^3$ $M^{-1}s^{-1}$, which is compatible with previous measurements of dsDNA association kinetics on surfaces[32] and 10^3 times smaller than the typical value in solution. [33]In the absence of **I**, the streptavidin-associated fluorescence remained unchanged over time. The active gel dynamics was significantly slower (Fig. 2B), with a characteristic time of 300 min, obtained by quantifying the standard deviation of the microtubule fluorescence over time. Fig. 2C (red) shows the titration of kinesins attached to the surface by increasing concentrations of **I**. We extracted an equilibrium constant $K_1 = 2.3 \times 10^{-2}$ for reaction (1), similar to the one measured in the absence of microtubules ($K^*_1 = 3.6\times10^{-2}$, SI Fig. S4) confirming that reaction (1) is driven by DNA hybridization and not by a potential kinesin-microtubule interaction. We estimated the corresponding equilibrium constant in solution at 22 °C to be 4×10^6 (NUPACK) indicating that reaction (1) is significantly hindered on the surface compared to solution, as expected.[34] Importantly, increasing [**I**] resulted in an increasingly contracted microtubule network (Fig 2C black) and we observed network structures from slightly contracted at 5 nM, to bright bands at 50 nM and strong focal contractions at ≥ 250 nM (SI Fig. S5).

Changing the length of the duplex in the complex **S**:**T**, which allows attaching kinesin clusters to the surface, provides another way to control the amount of kinesin clusters released in solution via the DSD reaction. To do so, **T** was truncated at the 3' end to make duplexes with 15, 22 and 30 bp that were displaced with [**I**] = 1 μM (Fig. 2D and Movie S2). The onset time of gel activity slightly increased with the increasing stability of duplex **S**:**T** and we measured 40, 50 and 80 min, respectively. In contrast, the final structure of the gel dramatically changed, with faint regular bands for the 30 bp-long duplex, bright bands with local gel breaks for 22 bp, and a strong global contraction, as the one observed above, for the 15 bp-long duplex. A third parameter that

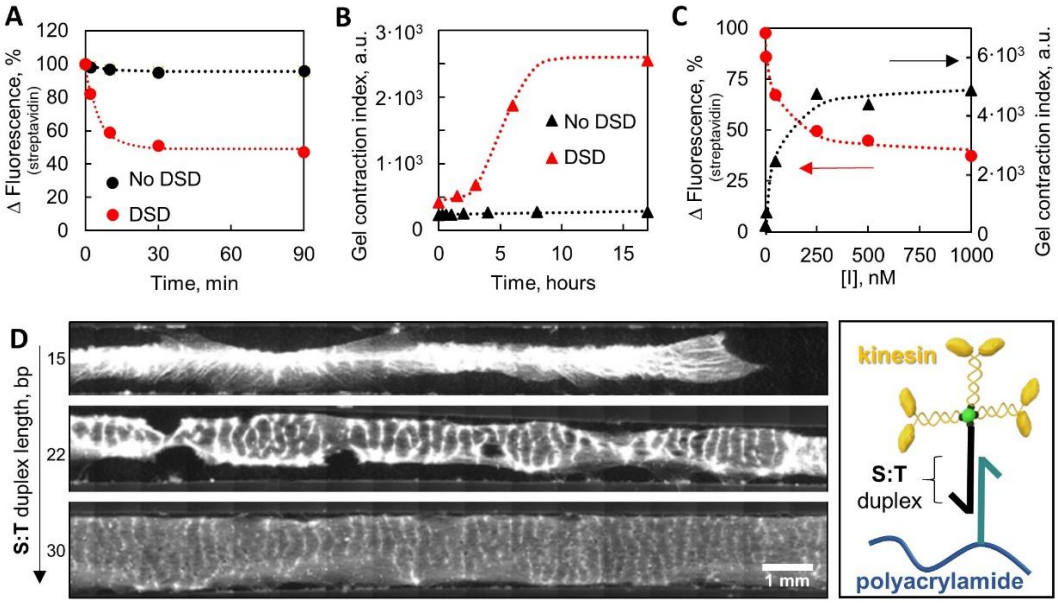

Figure 2: Influence of the kinetics and thermodynamics of the DSD reaction on the active gel patterning. Streptavidin fluorescence on the surface of the glass (A) and standard deviation of microtubules fluorescence (B) as a function of time in the presence of 1 μM of **I**. The dotted lines are fits to eqs. S2 and S8 respectively. Streptavidin fluorescence on the surface of the glass after 90 minutes (red) and standard deviation of microtubules fluorescence after 17 hours (black) as a function of the concentration of **I** (C). The dotted lines are fits to eqs. S6 and S7. D: Fluorescence microscopy images of microtubules confined in glass channels modified with biotinylated DNA strands of different complementarity lengths in the presence of 1 μM **I** strand after 18 hours. For detailed conditions see SI.

allows to control gel activity through DSD reaction is the concentration of the immobilized kinesin on the surface. Fig. S6 examines the effect of **str** surface density on the dynamics of the active gel for [**I**] = 1 μM. For the densities of 0.5 ×, 1 × and 2 × 10^{10} molecules/cm^2 we respectively observed: slight bulk contraction with no bands, weak bands and bright bands with strong global contraction. Taken together, the data from Fig. 2 and S4-S6 imply that the DSD reaction is fast compared to the dynamics of the active gel and that the state of the gel is determined by the concentration of motors released in solution, which is tuned by the thermodynamics of the DSD reaction and by the surface density of **str**.

In biology, morphogens play a crucial role in the patterning of developing tissues by diffusing in space and forming concentration gradients that provide positional information to downstream molecular events. In particular, morphogen gradients influence active matter processes in vivo.[1] In the following, we assessed the invader DNA strand as a morphogen that provides positional information to an active gel. To do so, 1μM of DNA **I** (the morphogen) was put solely on the left side of a channel filled with microtubules (Fig. 3). On this side of the channel the onset of gel activity was detected after two hours followed by the formation of bright spots and global contraction in the *y* direction. As expected, **I** diffused toward the right side forming a concentration gradient of **I**, and thus of released kinesin clusters, that contracted the gel with decreasing amplitude and increased delay as the distance from the injection point increased (Fig. 3 and Movie S3). In the central part of the channel, **I** arrived by diffusion at a concentration significantly lower than 1 μM, and activity was observed after 10 hours with a front of activity progressing from left to right, with bright bands appearing sequentially. No activity was observed over the course of 43 hours in the right side of the channel where the morphogen concentration was negligible.

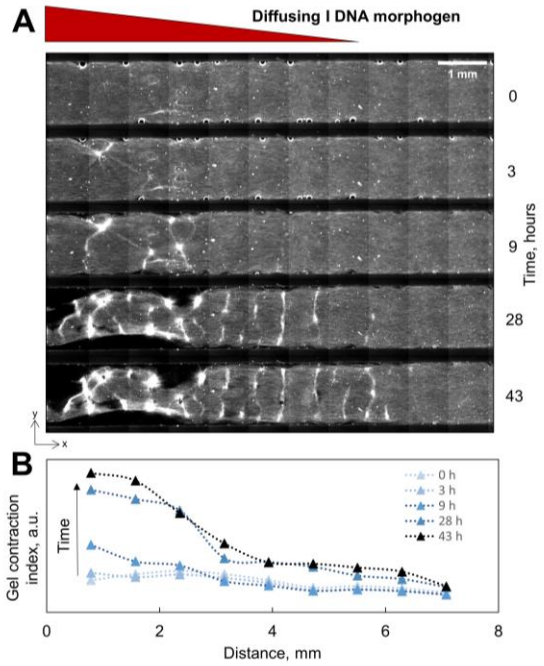

Figure 3: Active gel patterning through an underlying morphogen gradient of DNA A: Time-lapse fluorescent microscopy images of the microtubule solution confined in glass channels after the addition of 1 μM **I** DNA on the left side. For detailed conditions see SI. B: Standard deviation of microtubules fluorescence computed along the channel length for each time point. The dotted lines are guides to the eye.

The multiscale structuring of shapeless soft matter, including active materials, is conceptually and experimentally challenging. Here it was shown that the large-scale mechanical self-organization of microtubules could be activated in a programmable manner by a DNA signal. DNA-kinesin conjugates hybridized to a DNA-modified surface could be released in a controllable way by specific DNA inputs that trigger a DNA strand displacement reaction. Moreover, the DNA input could be distributed heterogeneously across space and act as a morphogen. transforming chemical information into a mechanical and structural output with spatial resolution. Complementary to the systems that utilize mechano-chemical transduction,[35] this work provides an approach allowing for preparation of a synthetic material that actuates along a chemo-mechanical pathway. We anticipate that this methodology will open a new route to accessing novel self-fabricated, force-exerting synthetic soft matter with the potential of integration in soft robotics and biological environments.

Funding Sources

We are also thankful for the financial support from the European Research Council (ERC) under the European's Union Horizon 2020 program (grant no. 770940, A.E.-T.) and by a Marie Sklodowska-Curie fellowship (grant no. 888997, Y.V.) from the European Union's Horizon 2020 Program.

REFERENCES

(1) Collinet, C.; Lecuit, T. Programmed and Self-Organized Flow of Information during Morphogenesis. *Nat. Rev. Mol. Cell Biol.* **2021**, *22* (4), 245–265.

(2) Hannezo, E.; Heisenberg, C. P. Mechanochemical Feedback Loops in Development and Disease. *Cell* **2019**, *178* (1), 12–25.

(3) Needleman, D.; Dogic, Z. Active Matter at the Interface between Materials Science and Cell Biology. *Nat. Rev. Mater.* **2017**, *2*.

(4) Senoussi, A.; Vyborna, Y.; Berthoumieux, H.; Galas, J.-C.; Estevez-Torres, A. Learning from Embryo Development to Engineer Self-Organizing Materials. In *Out-of-Equilibrium (Supra)molecular Systems and Materials*; Giuseppone, N., Walther, A., Eds.; WILEY-VCH GmbH, 2021; pp 21–60.

(5) Yurke, B.; Turberfield, A. J.; Mills, A. P.; Simmel, F. C.; Neumann, J. L. A DNA-Fuelled Molecular Machine Made of DNA. *Nature* **2000**, *406* (6796), 605–608.

(6) Qian, L.; Winfree, E. Scaling Up Digital Circuit Computation with DNA Strand Displacement Cascades. *Science (80-.).* **2011**, *332* (6034), 1196–1201.

(7) Zhang, D. Y.; Seelig, G. Dynamic DNA Nanotechnology Using Strand-Displacement Reactions. *Nat. Chem.* **2011**, *3*

(2), 103–113.
(8) Montagne, K.; Plasson, R.; Sakai, Y.; Fujii, T.; Rondelez, Y. Programming an in Vitro DNA Oscillator Using a Molecular Networking Strategy. *Mol. Syst. Biol.* **2011**, *7* (1), 466.
(9) Padirac, A.; Fujii, T.; Estévez-Torres, A.; Rondelez, Y. Spatial Waves in Synthetic Biochemical Networks. *J. Am. Chem. Soc.* **2013**, *135* (39), 14586–14592.
(10) Srinivas, N.; Parkin, J.; Seelig, G.; Winfree, E.; Soloveichik, D. Enzyme-Free Nucleic Acid Dynamical Systems. *Science (80-.).* **2017**, *358* (6369), eaal2052.
(11) Heinen, L.; Walther, A. Programmable Dynamic Steady States in ATP-Driven Nonequilibrium DNA Systems. *Sci. Adv.* **2019**, *5* (7), 32–37.
(12) He, L.; Mu, J.; Gang, O.; Chen, X. Rationally Programming Nanomaterials with DNA for Biomedical Applications. *Adv. Sci.* **2021**, *8* (8), 2003775.
(13) Vyborna, Y.; Vybornyi, M.; Häner, R. From Ribbons to Networks: Hierarchical Organization of DNA-Grafted Supramolecular Polymers. *J. Am. Chem. Soc.* **2015**, *137* (44), 14051–14054.
(14) Fern, J.; Schulman, R. Modular DNA Strand-Displacement Controllers for Directing Material Expansion. *Nat. Commun.* **2018**, *9* (1), 3766.
(15) Buchberger, A.; Simmons, C. R.; Fahmi, N. E.; Freeman, R.; Stephanopoulos, N. Hierarchical Assembly of Nucleic Acid/Coiled-Coil Peptide Nanostructures. *J. Am. Chem. Soc.* **2020**, *142* (3), 1406–1416.
(16) Zadorin, A. S.; Rondelez, Y.; Gines, G.; Dilhas, V.; Urtel, G.; Zambrano, A.; Galas, J.-C.; Estevez-Torres, A. Synthesis and Materialization of a Reaction–Diffusion French Flag Pattern. *Nat. Chem.* **2017**, *9* (10), 990–996.
(17) Jeon, S.-J.; Hauser, A. W.; Hayward, R. C. Shape-Morphing Materials from Stimuli-Responsive Hydrogel Hybrids. *Acc. Chem. Res.* **2017**, *50* (2), 161–169.
(18) Cangialosi, A.; Yoon, C.; Liu, J.; Huang, Q.; Guo, J.; Nguyen, T. D.; Gracias, D. H.; Schulman, R. DNA Sequence–Directed Shape Change of Photopatterned Hydrogels via High-Degree Swelling. *Science (80-.).* **2017**, *357* (6356), 1126–1130.
(19) Wollman, A. J. M.; Sanchez-Cano, C.; Carstairs, H. M. J.; Cross, R. A.; Turberfield, A. J. Transport and Self-Organization across Different Length Scales Powered by Motor Proteins and Programmed by DNA. *Nat. Nanotechnol.* **2014**, *9* (1), 44–47.
(20) Keya, J. J.; Suzuki, R.; Kabir, A. M. R.; Inoue, D.; Asanuma, H.; Sada, K.; Hess, H.; Kuzuya, A.; Kakugo, A. DNA-Assisted Swarm Control in a Biomolecular Motor System. *Nat. Commun.* **2018**, *9* (1), 453.
(21) Sato, Y.; Hiratsuka, Y.; Kawamata, I.; Murata, S.; Nomura, S. M. Micrometer-Sized Molecular Robot Changes Its Shape in Response to Signal Molecules. *Sci. Robot.* **2017**, *2* (4), eaal3735.
(22) Nédélec, F. J.; Surrey, T.; Maggs, A. C.; Leibler, S. Self-Organization of Microtubules and Motors. *Nature* **1997**, *389* (6648), 305–308.
(23) Sanchez, T.; Chen, D. T. N.; DeCamp, S. J.; Heymann, M.; Dogic, Z. Spontaneous Motion in Hierarchically Assembled Active Matter. *Nature* **2012**, *491* (7424), 431–434.
(24) Popkin, G. The Physics of Life. *Nature* **2016**, *529* (7584), 16–18.
(25) Duclos, G.; Adkins, R.; Banerjee, D.; Peterson, M. S. E.; Varghese, M.; Kolvin, I.; Baskaran, A.; Pelcovits, R. A.; Powers, T. R.; Baskaran, A.; Toschi, F.; Hagan, M. F.; Streichan, S. J.; Vitelli, V.; Beller, D. A.; Dogic, Z. Topological Structure and Dynamics of Three-Dimensional Active Nematics. *Science (80-.).* **2020**, *367* (6482), 1120–1124.
(26) Wu, K.-T.; Hishamunda, J. B.; Chen, D. T. N.; DeCamp, S. J.; Chang, Y.-W.; Fernández-Nieves, A.; Fraden, S.; Dogic, Z. Transition from Turbulent to Coherent Flows in Confined Three-Dimensional Active Fluids. *Science (80-.).* **2017**, *355* (6331), eaal1979.
(27) Senoussi, A.; Kashida, S.; Voituriez, R.; Galas, J.-C.; Maitra, A.; Estevez-Torres, A. Tunable Corrugated Patterns in an Active Nematic Sheet. *Proc. Natl. Acad. Sci.* **2019**, *116* (45), 22464–22470.
(28) Niemeyer, C. M.; Sano, T.; Smith, C. L.; Cantor, C. R. Oligonucleotide-Directed Self-Assembly of Proteins: Semisynthetic DNA—Streptavidin Hybrid Molecules as Connectors for the Generation of Macroscopic Arrays and the Construction of Supramolecular Bioconjugates. *Nucleic Acids Res.* **1994**, *22* (25), 5530–5539.
(29) Hager, R.; Arnold, A.; Sevcsik, E.; Schütz, G. J.; Howorka, S. Tunable DNA Hybridization Enables Spatially and Temporally Controlled Surface-Anchoring of Biomolecular Cargo. *Langmuir* **2018**, *34* (49), 15021–15027.
(30) Rehman, F. N.; Audeh, M.; Abrams, E. S.; Hammond, P. W.; Kenney, M.; Boles, T. C. Immobilization of Acrylamide-Modified Oligonucleotides by Co-Polymerization. *Nucleic Acids Res.* **1999**, *27* (2), 649–655.
(31) Simmel, F. C.; Yurke, B.; Singh, H. R. Principles and Applications of Nucleic Acid Strand Displacement Reactions. *Chem. Rev.* **2019**, *119*, acs.chemrev.8b00580.
(32) Gao, Y. Secondary Structure Effects on DNA Hybridization Kinetics: A Solution versus Surface Comparison. *Nucleic Acids Res.* **2006**, *34* (11), 3370–3377.
(33) Morrison, L. E.; Stols, L. M. Sensitive Fluorescence-Based Thermodynamic and Kinetic Measurements of DNA Hybridization in Solution. *Biochemistry* **1993**, *32* (12), 3095–3104.
(34) Irving, D.; Gong, P.; Levicky, R. DNA Surface Hybridization: Comparison of Theory and Experiment. *J. Phys. Chem.*

B **2010**, *114*, 7631–7640.
(35) Senoussi, A.; Galas, J.-C.; Estevez-Torres, A. Programmed Mechano-Chemical Coupling in Reaction-Diffusion Active Matter. *bioRxiv* **2021**, 2021.03.13.435232.

SUPPORTING INFORMATION

DNA-controlled Spatio-temporal Patterning of Active Matter

Contents

1. Methods 7

1.1. Oligonucleotides. 7

1.2. Kinesin and microtubules preparation 8

1.3. Glass modification 8

1.4. Channel assembly 8

1.5. Kinesin conjugation to the glass surface of the channel 8

1.6. Active gel experiments. 8

1.7. Kinetics and thermodynamics experiments in Fig. 2A and Fig. 2C (red) 8

1.8. Gradient experiment (Fig. 3). 9

1.9. Imaging. 9

2. Quantifying the density of the streptavidin on the surface 9

3. Evaluation of the specific attachment of proteins and DNA to the surface 10

4. Control experiments of DNA strand displacement reaction showing the influence of invader complementarity and the presence of the microtubules 11

5. Models for the kinetics and thermodynamics of the DSD reaction and for the kinetics of gel activation 11

5.1. Kinetics of the DSD reaction 11

5.2. Thermodynamics of the DSD reaction 12

5.3. Kinetics of gel activation 12

6. Experiments showing the influence of the invader DNA strand concentration 13

7. Experiments showing the influence of the initial streptavidin surface density 13

8. Movies 14

Bibliography 14

1. Methods

1.1. Oligonucleotides. All oligonucleotides used in this study were purchased HPLC-purified from biomers.net GmbH. The immobilized **S** strand is 35-nt long. DNA targets **T-30**, **T** and **T-15** have, respectively, sequences complementary to 30, 22, or 15 bases of **S,** with a 5-nt overhang at the 5' end. The invader **I** is fully complementary to **T-30**, both 35-nt long. Non-specific binding of the target DNAs was checked by using biotinylated non-complementary DNA **NT**. Non-specific DSD reaction was checked with fluorescently-labeled non-complementary DNA **N**. The sequences of the DNA are listed in Table S1.

Table S1. DNA sequences used in the study.

Name	Sequence	5' modification	3' modification
S	GGAGATGAAGGAGATGAGTAGGATGAGTAGATGGT	Acrydite	Phosphate
T-30	CCCACACCATCTACTCATCCTACTCATCTCCTTCA	biotin	Phosphate
T	CCCACACCATCTACTCATCCTACTCAT	biotin	Phosphate
T-15	CCCACACCATCTACTCATCC	biotin	Phosphate
I	TGAAGGAGATGAGTAGGATGAGTAGATGGTGTGGG	-	-
NT	GGAGATGAAGGAGATGAGTAGGATGAGTAGATGGT	biotin	Phosphate
N	CATTCGGTAGTTGGAGCTGGTGGACG	FAM	-

1.2. Kinesin and microtubules preparation. Biotin-labeled kinesin K401 was purified as described in ref. 1. Purified tubulin and rhodamine-labeled tubulin protein for microtubules preparation were bought from Cytoskeleton Inc. Taxol-stabilized microtubules were prepared as described in ref. 2 and were incubated at room temperature for at least 24 hours before using them in the experiments.

1.3. Glass modification. To prepare substrates for DNA immobilization, glass coverslips were first cleaned by sonication over 10 minutes in 0.5 % Hellmanex (Sigma), the same procedure was repeted in ethanol and finally, in 0.1 M KOH.[3] The slides were subsequently rinsed in water. Next, the glass slides were treated with silane-coupling solution (1% acetic acid and 0.5% 3-(Trimethoxysilyl)propylmethacrylate in ethanol) for 15 minutes and rinsed in water. 200 µl of an aqueous solution containing 2% acrylamide, 0.02% 5′-acrylamide oligonucleotide **S**, 0.125% w/v APS and 0.125% v/v TEMED was manually pipetted onto silanized slides. The solution was covered with a second silanized coverslip, making a sandwich, and placed in a water-saturated, argon atmosphere inside a desiccator; at room temperature for 3 hours to allow polymerization. Non-immobilized DNA and polyacrylamide were removed from the surface by washing in water, then air-dried and stored at room temperature. The calculated maximum surface density of **S** in this DNA-modified glass slide was $7 \cdot 10^{13}$ mol/cm^2.

1.4. Channel assembly. Channels were assembled using a DNA-modified glass slide (26 × 75 × 1 mm) and a DNA-modified coverslip (22 × 60 × 0.17 mm) separated by Parafilm cut with a Graphtec Cutting Plotter CE6000-40, gently melted over a heating plate. The 22×1.5×0.1 mm^3 fabricated channel had a volume of ~ 3.5 µL and a coated surface of ~ 0.7 cm^2.

1.5. Kinesin conjugation to the glass surface of the channel. Before each experiment, channels were treated with a 2% solution of Pluronic127 in 1x PBS at room temperature in a humid chamber for one hour to block unspecific protein adsorption and subsequently washed with 50 µl of 1x PBS (in both directions). To create a final concentration of kinesin clusters on the surface equal to 1×10^{10} molecules/cm^2, 10 µl of a 20 nM solution of biotin-labeled complementary DNA (**T**, **T-15**, or **T-30**) in 1x PBS was flushed through each channel and allowed to hybridize to the surfaces for one hour at 65 °C in a humid chamber placed on the heating plate. After the subsequent washing with 50 µl of 1x PBS (in both directions), 10 µl of the 20 nM solution of Atto 488-tagged streptavidin **str** (Sigma-Aldrich) was added and incubated at RT for 10 min. Non-conjugated streptavidin was washed with 50 µl of 1x PBS (in both directions). Lastly, 10 µl of 50 nM of biotin-labeled kinesin (K401) **kin** in 1x PBS was added to each channel and incubated for 15 min at RT to conjugate to the surface-immobilized streptavidin/DNA constructs. The excess of the kinesin was washed with 50 µl of 1x PBS (in both directions), and the channels were used immediately for further experiments.

1.6. Active gel experiments. After the kinesin conjugation, 4 µl of the microtubules solution with the required concentration of the components as indicated in Table S2 was filled in the channel by capillarity and sealed with vacuum grease and placed on specimen holder (with or without temperature control) the microscope scanning stage (in case of holder with temperature control: mineral oil was added between the glass channels and the thermoplate of the microscope. The type of the holder did not have any effect on the experiment).

1.7. Kinetics and thermodynamics experiments in Fig. 2A and Fig. 2C (red). To track the changes of the fluorescence of the streptavidin on the surface, the channels were filled with solutions (Table S2) and were left open to enable

subsequent washing. After the incubation time indicated in Table S2, the channels were washed with 50 µl of 1x PBS and the fluorescence was recorded.

1.8. Gradient experiment (Fig. 3). To create a non-homogeneous concentration profile of I DNA inside the channel, and thus mimic the morphogen gradients that provide positional information to downstream molecular events in biology, ~25% (0.75 µl) of the functionalized channel was filled with a solution of microtubules containing 1 µM **I** DNA (the remaining volume was filled with a solution of microtubules without **I** DNA). Once sealed, the **I** DNA was let to diffuse in the confined environment of the glass channel.

1.9. Imaging. Epifluorescence images of the channels were obtained at 22°C with a Zeiss Observer 7 automated microscope equipped with a Hamamatsu C9100-02 camera, a 10× objective, and a motorized stage controlled with MicroManager 1.42. Images were recorded with excitations at 470 or 550 nm with a CoolLED pE2. ***Image Analysis*** was done with ImageJ. To estimate the gel contraction, we defined a gel contraction index as follows: first, a Gaussian filter was applied to the microtubule images, then the standard deviation of the microtubule intensity was calculated. A local gel contraction index was obtained considering a region of interest in the images.

Table S2. Summarized experimental conditions. *

	Fig 1C	Fig. 2A										Fig 2B		Fig. 2C red						Fig. 2C black						Fig.2 D			Fig 3A
Biotin-DNA	T	T										T		T												T-15	T	T-30	T
str, molecules/cm2	5×10^9	5×10^9										5×10^9		1×10^{10}												1×10^{10}			1×10^{10}
I DNA, nM	1000	1000	Ø	1000	Ø	1000	Ø	1000	Ø	1000	Ø	1000	Ø	Ø	5.0	50	250	500	1000	Ø	5.0	50	250	500	1000	1000			0.75 ul of 1000
Incubation time, min	1020	2	2	10	10	90	90	180	180	1140	1140	1020	1020	90						1020						1080			2580
Microtubules, mg/ml	0.25	Ø										0.25	0.25	0.25						0.25						0.25			0.25

	Fig. S1A	Fig. S1B	Fig. S2A	Fig. S2B	Fig. S2C	Fig. S3A	Fig. S3B	Fig. S3C	Fig. S4											
Biotin-DNA	T	T	NT	Ø	T	T			T											
str, molecules/cm2	Variable	Variable	0	0	2×10^{10}	1×10^{10}			1×10^{10}											
I DNA, nM	Ø	Ø	Ø			Ø	1000	N DNA 1000	Ø	5.0	50	250	500	1000	Ø	5.0	50	250	500	1000
Incubation time, min	Ø	Ø	Ø			1200			90											
Microtubules, mg/ml	Ø	Ø	Ø			0.25			Ø						0.25					

	Fig. S4												Fig. S5						Fig.S6				Movie S1 top	Movie S1 bottom	Movie S2	Movie S3
Biotin-DNA	T												T						T-30				T	As in Fig. 1C	As in Fig. 2D	As in Fig. 3
str, molecules/cm2	1×10^{10}												1×10^{10}						1×10^{10}	5×10^9	1×10^{10}	2×10^{10}	1×10^{10}			
I DNA, nM	Ø	5.0	50	250	500	1000	Ø	5.0	50	250	500	1000	Ø	5.0	50	250	500	1000	Ø	1000	1000	1000	Ø			
Incubation time, min	90												600						1020				1020			
Microtubules, mg/ml	Ø						0.25						0.25						0.25				0.25			

*In addition, working solution was composed of 1× PEM buffer, (80 mM PIPES, 1 mM EGTA, 1 mM $MgSO_4$, 130 mM KOH) 10 mM K-acetate, 10 mM KCl, 5 mM MgCl2, 2% (wt/vol) Pluronic F-127, 5 µg/mL creatine kinase, 20 mM creatine phosphate, 20 µM taxol, 2 mM ATP, 1 mg/mL BSA, 1 mM trolox, 20 mM D-glucose, 3 mM DTT, 150 µg/mL glucose oxidase, 25 µg/mL catalase. "Incubation time" refers to the duration of the experiment.

2. Quantifying the density of the streptavidin on the surface

We estimated the average surface density of streptavidin for each experiment by using fluorescently-labeled **str**. Glass channels with hybridized biotin-tagged DNA were filled with the solutions of the fluorescently-labeled streptavidin with concentrations ranging from 0 to 50 µM and we recorded the fluorescence signal before the washing step from which we subtracted background fluorescence to obtain F_{bw}. We obtained a linear relation that we fitted with $F_{bw} = a[\mathbf{str}]_{bulk}$. Then, the channels were washed with 50 µl PBS buffer and the fluorescence was recorded again, noted F_{aw}. We then calculated the equivalent concentration of **str** on the surface as $[\mathbf{str}]_{surf} = (F_{aw})/a$, and the corresponding surface density considering the volume (3.5 µL) and the surface of the channel (0.7 cm2). The obtained results were

converted to coverage of streptavidin (in molecules/cm^2) by dividing this result by the surface of the channel. A control experiment with surfaces lacking the biotinylated **S** strand indicated that the non-specific binding of **str** to the surface was negligible.

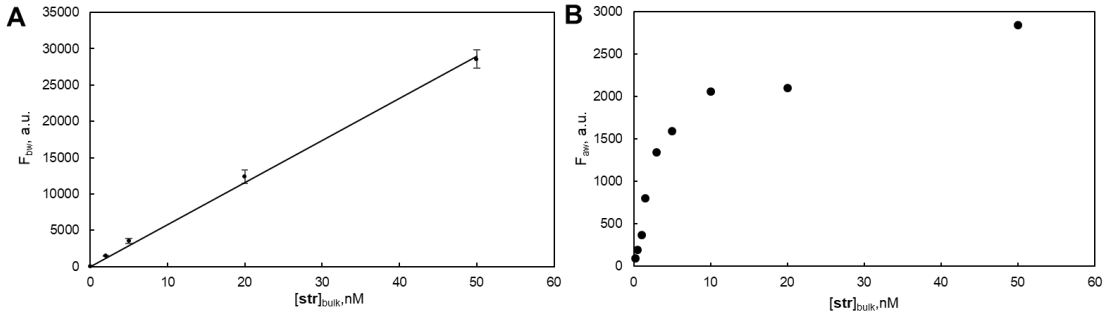

Figure S1. A: Fluorescence intensity before washing as a function of streptavidin concentration in bulk. The data points and error bars correspond, respectively, to the averages and standard deviations obtained from a triplicate. The line is a linear fit to the data. B: Fluorescence intensity after washing as a function of streptavidin concentration in bulk.

3. Evaluation of the specific attachment of proteins and DNA to the surface

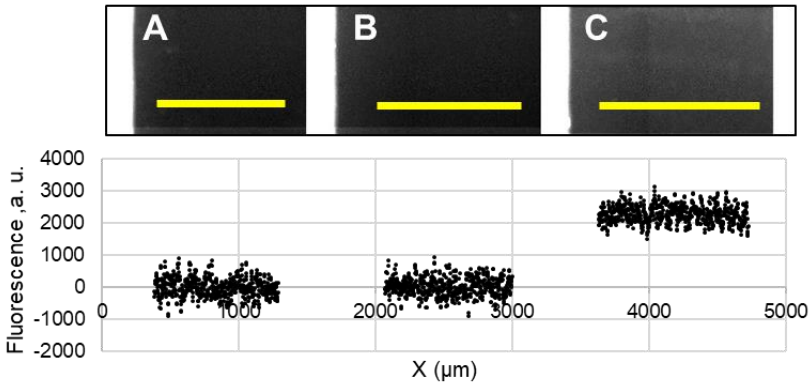

Figure S2: Top: Fluorescence images of the surfaces treated with 20 nM of non-complementary biotinylated **NT** DNA (A), no DNA (B), and 20 nM complementary biotinylated **T** DNA (C) and subsequently treated with 20 nM fluorescently-labeled streptavidin for 10 min and washed with buffer. Bottom: fluorescence intensity profiles along the yellow line depicted in the top figures. The results indicate a selective attachment between the **T** and the DNA-modified surface. Control surfaces did not show signs of non-specific adsorption of streptavidin or biotinylated DNA.

4. Control experiments of DNA strand displacement reaction showing the influence of invader complementarity and the presence of the microtubules

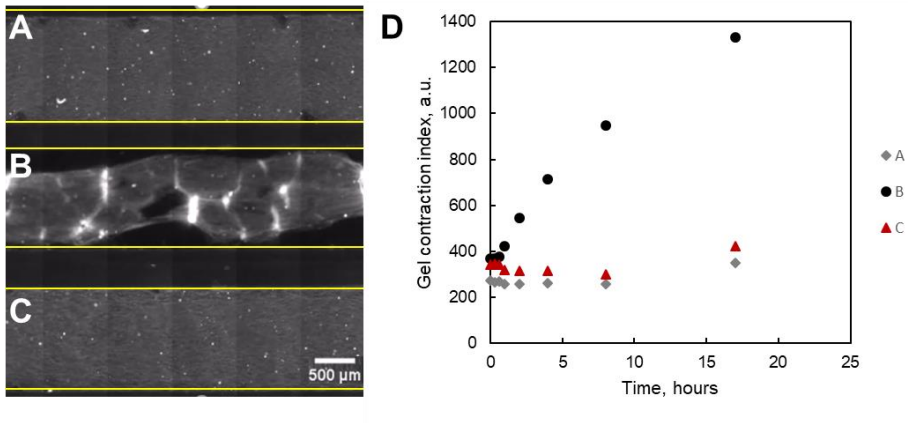

Figure S3: The kinesin-decorated surfaces are stable in the absence of complementary DNA **I**. Microtubule fluorescence images after 20 h for [**I**] = 0 (A), [**I**] = 1 µM (B) and [**N**] = 1 µM (C). No activity was observed in the presence of non-complementary DNA **N** (C). The borders of the channels are marked in yellow. D: Corresponding standard deviation over time of the microtubule fluorescence for the data described in panels A-C. For detailed conditions see Table S2.

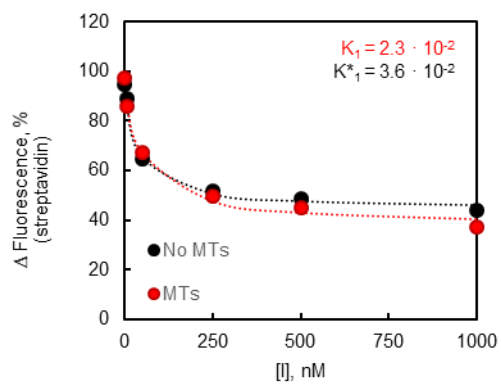

Figure S4: The release of **str** from the surface by **I** is independent of the presence of microtubules. **Str** fluorescence on the surface of the glass after 90 minutes for different concentrations of **I** in the presence (red) and in the absence (black) of microtubules. Equilibrium constants K_1 and K^*_1 of reaction (S1) were found by fitting the data to the equation S6.

5. Models for the kinetics and thermodynamics of the DSD reaction and for the kinetics of gel activation

5.1. Kinetics of the DSD reaction

We measured the detachment of the kinesin–streptavidin-DNA construct from the surface due to the DSD reaction in the presence of **I** by following the fluorescence intensity of **str** on the surface of the glass. We can write:

$$\mathbf{S}:\mathbf{T}:\mathbf{str}:\mathbf{kin} + \mathbf{I} \rightarrow \mathbf{S} + \mathbf{I}:\mathbf{T}:\mathbf{str}:\mathbf{kin} \qquad \text{(S1)}$$

Because **I** is in excess relative to **S**:**T**:**str**:**kin**, we can consider reaction (S1) as pseudo-first-order with an apparent rate constant $\kappa_1 = k_1[\mathbf{I}]_0$, with $[\mathbf{I}]_0$ = 1 µM in our experiments. We note **Y** = **S**:**T**:**str**:**kin**, and thus

$$[\mathbf{Y}](t) \rightarrow [\mathbf{Y}]_0 e^{-\kappa_1 t} \qquad \text{(S2)}$$

where the index 0 denotes the initial condition. In our experimental conditions, the change in fluorescence at the glass surface is expected to be $F(t) = \alpha[\mathbf{Y}](t)+F_{bk}$, where α is a constant related to the fluorescence quantum yield of species **Y** that, in addition, integrates the intensity of the excitation light and the performance of the microscope optics and camera, and F_{bk} is the background fluorescence measured in the channel in the presence of buffer. As a result, to extract κ_1, we normalize the fluorescence signal over time, $F(t)$, (data in Figs. 2A and S4) and fit it with:

$$\frac{F(t)}{F(0)} = ae^{-\kappa_1 t} + b \qquad \text{S2}$$

5.2. Thermodynamics of the DSD reaction

We note **Z** = **I:T**:**str**:**kin** and thus reaction (1) in the Main Text now writes

$$\mathbf{Y} + \mathbf{I} \rightleftharpoons \mathbf{S} + \mathbf{Z} \qquad \text{(S3)}$$

The equilibrium constant associated to the forward reaction is

$$K_1 = \frac{[\mathbf{S}][\mathbf{Z}]}{[\mathbf{Y}][\mathbf{I}]} = \frac{[\boldsymbol{Z}]^2}{([\mathbf{Y}]_0 - [\mathbf{Z}])([\mathbf{I}]_0 - [\mathbf{Z}])} \approx \frac{[\boldsymbol{Z}]^2}{([\mathbf{Y}]_0 - [\mathbf{Z}])([\mathbf{I}]_0)} \qquad \text{(S4)}$$

where the rightmost approximation is taken because species **I** is in excess. By solving the second-order polynomial, we find

$$[\mathbf{Z}] = \frac{1}{2}\left(-K_1[\mathbf{I}]_0 + \sqrt{(K_1[\mathbf{I}]_0)^2 + 4K_1[\mathbf{I}]_0[\mathbf{Y}]_0}\right) \qquad \text{(S5)}$$

With $[\mathbf{Y}] = [\mathbf{Y}]_0$-$[\mathbf{Z}]$ and the relation between $[\mathbf{Y}]$ and fluorescence F remaining valid, we have

$$F([\mathbf{I}]_0) = \alpha\left([\mathbf{Y}]_0 - \frac{1}{2}\left(-K_1[\mathbf{I}]_0 + \sqrt{(K_1[\mathbf{I}]_0)^2 + 4K_1[\mathbf{I}]_0[\mathbf{Y}]_0}\right)\right) + F_{bk} \qquad \text{(S6)}$$

which we fitted to data of the **str** fluorescence on the surfaces as a function of [**I**] in (Fig. 2C red disks and Fig. S4) to extract K_1.

Furthermore, if we suppose that that gel contraction index is proportional to [**Z**], the corresponding data as a function of [**I**] (Fig. 2C black triangles) was fitted to the equation:

$$F([\mathbf{I}]_0) = \alpha\left(\frac{1}{2}\left(-K_1[\mathbf{I}]_0 + \sqrt{(K_1[\mathbf{I}]_0)^2 + 4K_1[\mathbf{I}]_0[\mathbf{Y}]_0}\right)\right) + F_{bk} \qquad \text{(S7)}$$

5.3. Kinetics of gel activation

Fig. 2B in the Main Text shows the dynamics of the gel activation after the addition of DNA **I**. To extract a gel contraction rate, we heuristically fitted the data with the sigmoid equation

$$\mathrm{G} = \frac{a}{1 + e^{-k_g(t-t_0)}} + b \qquad \text{(S8)}$$

where G is the gel contraction index, calculated from the standard deviation of the fluorescence intensity of the microtubules, k_g is the rate constant associated to the contraction dynamics, t_0 a delay associated to the saturation process of the contraction (due either to resource depletion or a force equilibration between active contraction forces and the passive rigidity of the gel) and a and b are constants associated to the initial and final level of the gel contraction index. For Fig. 2B, we obtained $k_g = 60$ min^{-1} and $t_0 = 300$ min.

6. Experiments showing the influence of the invader DNA strand concentration

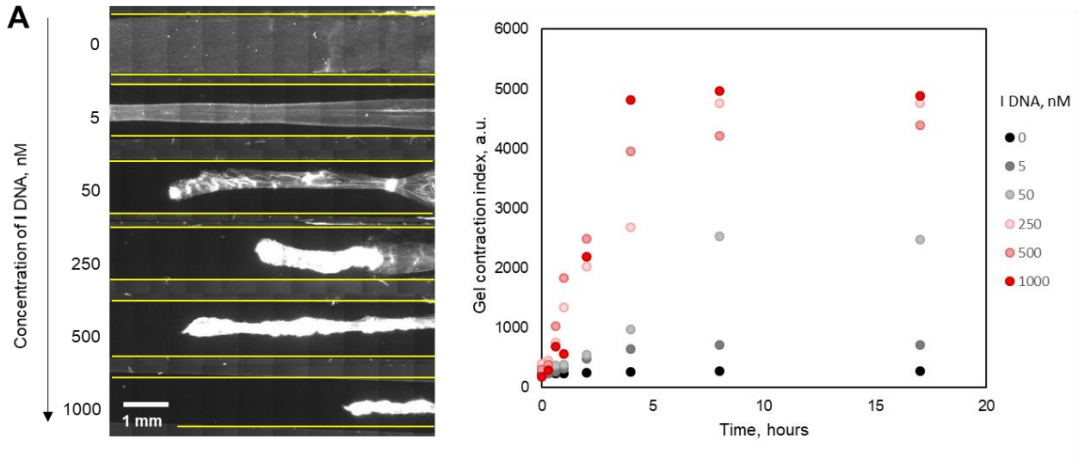

Figure S5: A: Fluorescence microscopy images of the microtubules-containing solution confined in glass channels 10 hours after the addition of the different concentrations of **I** strand. The borders of the channels are marked yellow. B: Corresponding standard deviation over time of the microtubule fluorescence. For detailed conditions see Table S2.

7. Experiments showing the influence of the initial streptavidin surface density

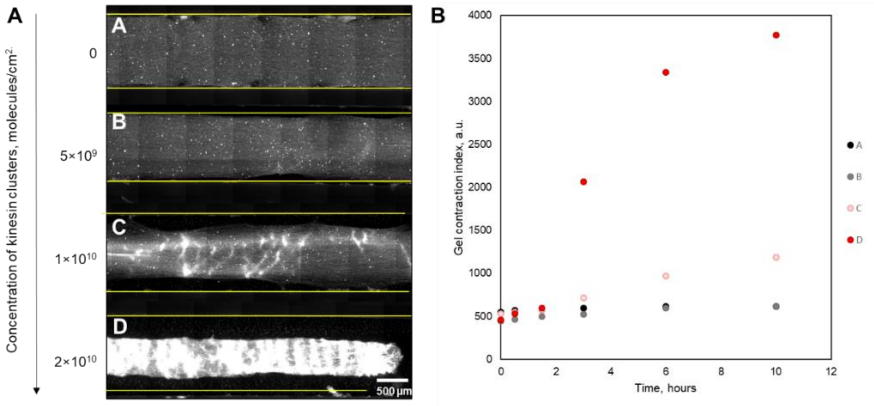

Figure S6: A: Fluorescence microscope images of the microtubule-containing solution confined in glass channels in the absence (A) and in the presence of 1 µM **I** DNA (B, C, D) at different streptavidin surface densities: 5×10^9 (B), 1×10^{10} (A and C), and 2×10^{10} molecules/cm^2 (D). The borders of the channels are marked yellow. The images were recorded 17 hours after the addition of **I**. B: Corresponding standard deviation over time of the microtubule fluorescence. For detailed conditions see Table S2.

8. Movies

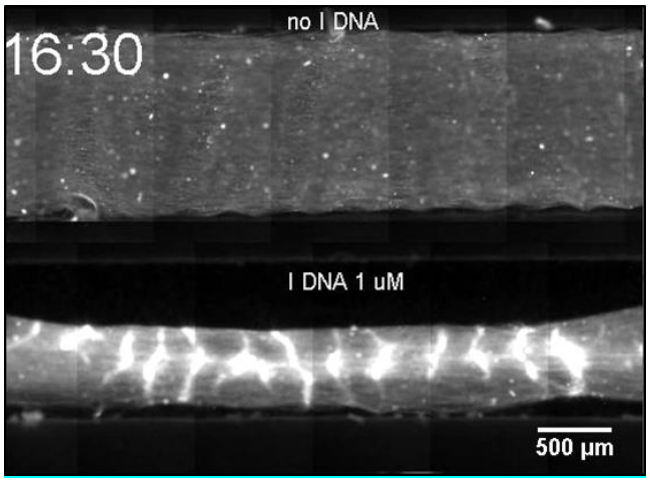

Movie S1. Fluorescent microscopy images of the microtubule solution confined in glass channels in the absence (top) and in the presence of 1 µM of **I** DNA (bottom).

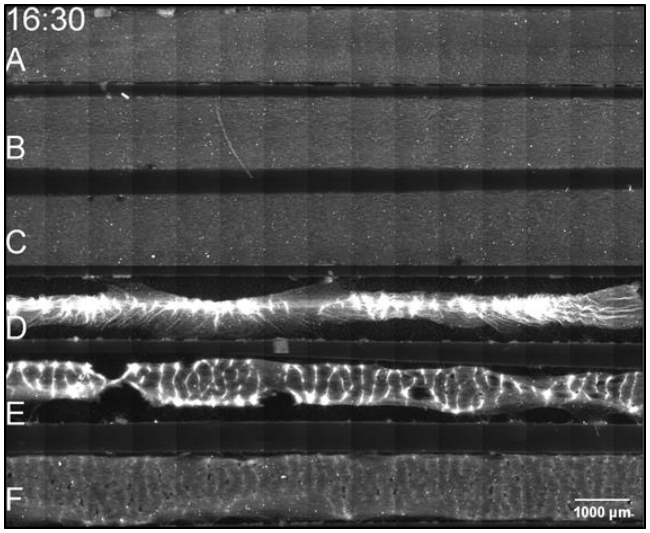

Movie S2. Fluorescence microscopy images of the microtubule solution confined in glass channels modified with biotinylated DNA strands of different complementarity length (15 nt (A and D); 22 nt (B and E); 30 nt (C and F)) in the absence (A-C) and in the presence (D-F) of 1 µM **I** strand. The shadows moving through the images are the artifacts due to the air bubbles in the oil separating glass slide and the temperature controlled stage.

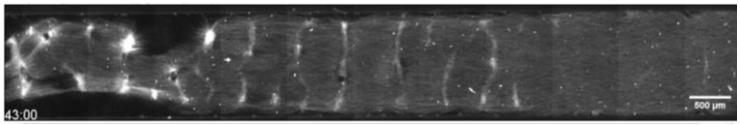

Movie S3. Fluorescence microscopy images of the microtubule solution confined in glass channels after the addition of 0.75 uL of 1 µM **I** DNA on the left-hand side.

Bibliography

(1) Subramanian, R.; Gelles, J. Two Distinct Modes of Processive Kinesin Movement in Mixtures of ATP and AMP-PNP. *J. Gen. Physiol.* **2007**, *130* (5), 445–455.

(2) Senoussi, A.; Kashida, S.; Voituriez, R.; Galas, J. C.; Maitra, A.; Estevez-Torres, A. Tunable Corrugated Patterns in an Active Nematic Sheet. *Proc. Natl. Acad. Sci. U. S. A.* **2019**, *116* (45), 22464–22470.

(3) Sanchez, T.; Dogic, Z. *Engineering Oscillating Microtubule Bundles*, 1st ed.; Elsevier Inc., 2013; Vol. 524.